Contents list available at CBIORE journal website

International Journal of Renewable Energy Development

Journal homepage: https://ijred.cbiore.id

Research Article

Cotton-derived biochar fibers modified by doping Al_2O_3 and $MgSO_4$ for application to hydrogen storage

Sumrit Mopoung* and Wanvilai Singse

Chemistry Department, Faculty of Science, Naresuan University, Phitsanulok, Thailand.

Abstract. Biochar fiber and activated biochar fibers from cotton fiber were prepared by carbonization at 400-700°C and activation with 5 wt.% Al_2O_3 and $MgSO_4$, respectively. The final products were characterized by BET, FTIR, XRD, and SEM-EDS. The hydrogen storage of the final products at 1.5 bar pressure and room temperature was studied. The objective of this research was to study the effects of Al_2O_3 or $MgSO_4$ on activation and doping of Al or Mg compounds on cotton fibers and hydrogen storage of products at low pressure and room temperature. The results showed that the surface areas, micropore volumes, and average pore sizes developed well with increasing carbonization temperatures from 400°C to 700°C. In addition, the surface functional groups such as OH, C=O, COOH and C-O-C were also more developed with increasing carbonization temperature. Furthermore, the results confirmed that MgO or Al_2O_3 accumulated on the surface of the composites. The results of hydrogen storage showed that hydrogen uptake capacity due to spillover mechanism increased with increasing of carbonization temperature from 400°C to 700°C during the preparation of biochar fiber and activated biochar fibers. The hydrogen capacity at room temperature and 1.5 bar fell within the range of 0.32-0.44 wt.%, 0.45-0.52 wt.%, and 0.59-0.63 wt.% for biochar fiber, Mg-activated biochar fibers, and Al-activated biochar fibers, respectively. This is because hydrogen molecules bonded on the surface of the products with physisorption. Therefore, hydrogen desorbs even at low temperature. It was concluded that metal biochar fibers made from cotton fiber with doping and activation by Al_2O_3 and $MgSO_2$ at 400-700°C are candidate adsorbers for hydrogen storage under 1.5 bar and room temperature with fast kinetics (within 30 min), quite high sorption selectivity/capacity (up 0.63 wt.%), and sorption stability/reversibility (at room temperature and 80°C).

Keywords: Cotton fiber; Activated biochar fiber; Aluminium oxide; Magnesium sulphate; Hydrogen storage

Received: 4th Feb 2025; Revised: 25th March 2025; Accepted: 6th April 2025 ; Available online: 9th April 2025

1. Introduction

Metal-carbon materials have specific mechanical, optical, electronic, or physical properties (Lee, 2020). These materials have been employed in hydrogen production and storage or the methanation reaction of carbon monoxide/dioxide, photocatalysis, environmental remediation (Buaki-Sogó *et al.*, 2020), and energy storage (Xiao *et al.* 2023). The doping of metals on porous carbon materials changes the energy stripe structure and electron transfer characteristics, along with the surface polarity of carbon-based materials (Yao *et al.*, 2022) and also improves the degree of graphitization, and provides more active sites with uniformly distributed high-density active sites (Xiao *et al.*, 2023). For instance, Co, Ni, Fe, or Cu - carbon nanocomposites, which carbonized and reduced from a carbon matrix precursor of polyvinyl chloride, showed up to 50 layers of core metals with 20-100 nm size (Kryazheva *et al.*, 2019). Generally, activated carbon and biochar (BC), which are abundant in nature and exhibiting porous structure and tunable surface chemistry, have emerged as an ideal support for the dispersion of active metals for electrocatalysis (Buaki-Sogó *et al.*, 2020). For example, a catalytic system of platinum nanoparticles dispersed on cotton carbon nanofiber support was used for nitro reduction catalysis (Yao *et al.*, 2022). The Cu, Co, Mn - activated carbons have been used for the conversion of nitrite to nitrates and ammonium (Gutsanu *et al.*, 2023). However, the development of low-cost, scalable, industrially and economically attractive, and sustainable carbon material preparation methods is a continued need (Lan *et al.*, 2021). Therefore, the use of activated carbons or BC from biomass origins is a step forward in the development of more sustainable processes enhancing material recycling and reuse in the frame of a circular economy (Buaki-Sogó *et al.*, 2020). Natural fibers, such as jute, cotton, flax, sisal, and hemp, which have low specific density, low cost, high strength, high sustainability, and decreased tool wear, possess crucial characteristics for polymeric composite materials preparation (Zaghloul *et al.*, 2021). Cotton fiber (CF) is a natural fiber of the purest form of cellulose, with around 90 % cellulose content (Awais *et al.*, 2021). This fiber possesses a multi layered structure containing crystalline cellulose fibrils (Zaghloul *et al.*, 2021). Its hollow nature is also good for its use as absorbent fibers (Awais *et al.*, 2021). Cotton-derived biochar has been used for soil restoration and carbon sequestration with high performance in commercial production (Tao *et al.*, 2024). However, it has never appeared for hydrogen storage (HS) via metal supporting. Therefore, the CF is used for the preparation of metals-biochar fibers for HS in this research. Furthermore, biochar-based functional materials offer many advantages due to their tunable porosity and surface

* Corresponding author
Email: sumritm@nu.ac.th (S. Mopoung)

https://doi.org/10.61435/ijred.2025.61128
ISSN: 2252-4940/© 2025.The Author(s). Published by CBIORE

area, which have been widely used in the preparation of nanostructured composites that can be applied as materials for energy storage and conversion (Buaki-Sogó *et al.*, 2020). Hydrogen can replace fossil fuels by achieving both high energy effectiveness and eco-friendliness because of its high gravimetric energy density and pure byproducts (Hwang *et al.*, 2021). It produces energy without CO_2 emissions making hydrogen an interesting energy source for stationary and vehicular applications (Buaki-Sogó *et al.*, 2020). Incorporation of metal particles into carbon can dissociate hydrogen and enhance hydrogen adsorption capacity (Xu *et al.*, 2024). For example, Pd-decorated carbon from sepiolite exhibited a storage capacity 4 times higher than the raw material without Pd doping at room temperature (Buaki-Sogó *et al.*, 2020). Doping of 2.5 wt.% Pd in the carbon pristine material and 5.1 wt.%. Ni in graphite nanofibers could increase the HS capacity of 0.13 wt.% and 2.2 wt.% at room temperature, respectively (Sharon *et al.*, 2011). In another example, a Pd-activated carbon fiber could achieve 0.31 wt.% HS at 77 K and 10 MPa (Hwang *et al.*, 2021). However, one factor that needs to be considered is the type of metal for reducing the cost of the metal-carbon material production. Aluminum and magnesium are cheap and abundant elements, which offer low weight per electron exchanged, small size, and high charge (Hirscher *et al.*, 2020). Al_2O_3 and MgO have been supported on monoxides or acidic zeolites (Bettahar, 2024). Al_2O_3 has been doped on MgO (Shun *et al.*, 2024) and multi-walled carbon nanotubes (Konni & Mukkamala, 2019), respectively. Including, MgO has been supported on carbon nanofiber (Khafidz *et al.*, 2019). These materials have been used for hydrogen storage at high pressure and low temperature, which are difficult to use in practical applications. However, the Al_2O_3 and MgO have also never appeared for supporting on biochar or activated biochar, especially cotton derived activated biochar fiber. Including, many previous researches have studied hydrogen adsorption at high pressure and low temperature. In this study, low pressure and room temperature conditions were used to reduce cost and ease of operation. Therefore, Al and Mg were used for cotton derived activated biochar fiber (CABF) preparation for hydrogen storage at low pressure and room temperature.

The purpose of this research was to study the effects of Al_2O_3 or $MgSO_4$ on activation and doping of Al or Mg compounds on cotton fibers at carbonization temperatures of 400°C to 700°C and to investigate the HS of final products at room temperature and low pressure. The products were characterized by proximate analysis, BET, FTIR, XRD, and SEM-EDS. Finally, the hydrogen adsorption experiments with the manufactured biochar fiber and metal-biochar fiber products were carried out at 1.5 bar pressure and room temperature.

2. Materials and Methods

2.1 Preparation and Characterization of biochar fiber and activated biochar fiber

CF was dried in an oven (SL 1375 SHEL LAB 1350FX) at 105°C for 6 h. Dried CF was kept in a desiccator for further experiments. Proximate analysis of dried CF was carried out to determine fixed carbon, volatile matter, and ash content using the ASTM D 3172-13 (2021), ASTM D 5832-98 (1998), and ASTM D 2866-11 (2011) methods, respectively. Meanwhile, 20 g of CFs and 5 wt.% of Al_2O_3 or $MgSO_4$ (weight by Sartorius ED224s Germany) were mixed with distilled water in a ceramic crucible with three repetitions. The correction of 5 wt.% of Al_2O_3 or $MgSO_4$ attributed to the reducing of surface area of the bead

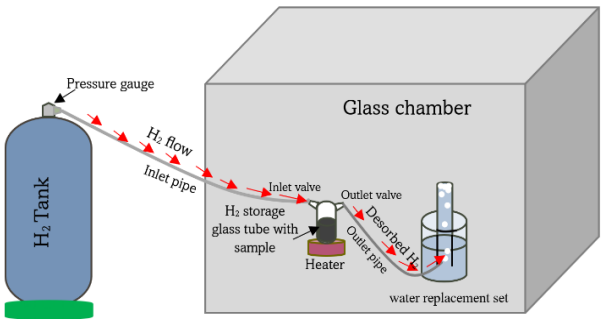

Fig 1. The chamber used for hydrogen adsorption experiments.

activated carbon with 7.6 wt.% by report of Nguyen *et al.* (2023). The mixed samples were dried in an oven at 105°C for 6 h. Subsequently, carbonization at 400°C-700°C with the heating rate of 10°C/min and soaking for 1 h in a muffle furnace (Fisher Scientific Isotemp® Muffle furnace U.S.A) under air atmosphere (partial air oxidation) with closing the lid of the crucible was performed. After completion, the sample products were cooled to room temperature and weighted for percent yield calculation. The final products were characterized by proximate analysis, BET at -196.15°C (Micromeritics TriStar II3020, Bavaria, Germany), FTIR between 400 cm^{-1} and 4000 cm^{-1} (Spectrum GX, Perkin Elmer, Connecticut, USA), XRD (PW 3040/60, X' Pert Pro Console, Philips, Netherland), and SEM-EDS (Leo1455VP Electron Microscopy, Cambridge, England).

2.2 Hydrogen storage

A sample (20 g) of biochar fiber (BCF) or CABFs was dried at 105°C overnight to remove any adsorbed gases and moisture and then cooled to room temperature. Each sample was used for hydrogen adsorption experiment with three repetitions, which was performed in a conventional static volumetric adsorption Pyrex glass apparatus (Fig 1.) following the method of Souvakon *et al.* (2011). The glass apparatus with samples was placed in the chamber. The air in the chamber was removed by replacing it with nitrogen gas in 2-3 cycles for oxygen removal. After that, hydrogen gas (ultrapureplus grade, 99.9999%) was flowed into the glass apparatus with samples for 30 minutes at a pressure of 1.5 bar and room temperature. The efficient of H_2 physisorption on micropore (Bader *et al.*, 2018) of product materials is focus. Finally, adsorbed hydrogen was desorbed from the samples at 80°C by heater. The volume of adsorbed hydrogen gas was measured by water replacement. The number of moles of hydrogen gas and the weight percent (wt.%) were calculated.

3. Results and discussion

3.1. Porous properties of products

Surface areas (Fig 2.A), pore volumes (Fig 2.B), and micropore volumes (Fig 2.D) of the CBCFs and metals-CABFs increased with increasing carbonization temperatures from 400°C to 700°C, while the average pore sizes show the opposite trend. The values of these parameters for the metal-CABFs are higher than the values for the CBCFs at each temperature [(Figs 2.A(a-c), 2.B(a-c), and 2.D(a-c)]. This order is inverted for the average pore size values [(Fig 2.C(a-c)]. This showed that the effects of carbonization temperature and metal compounds on the

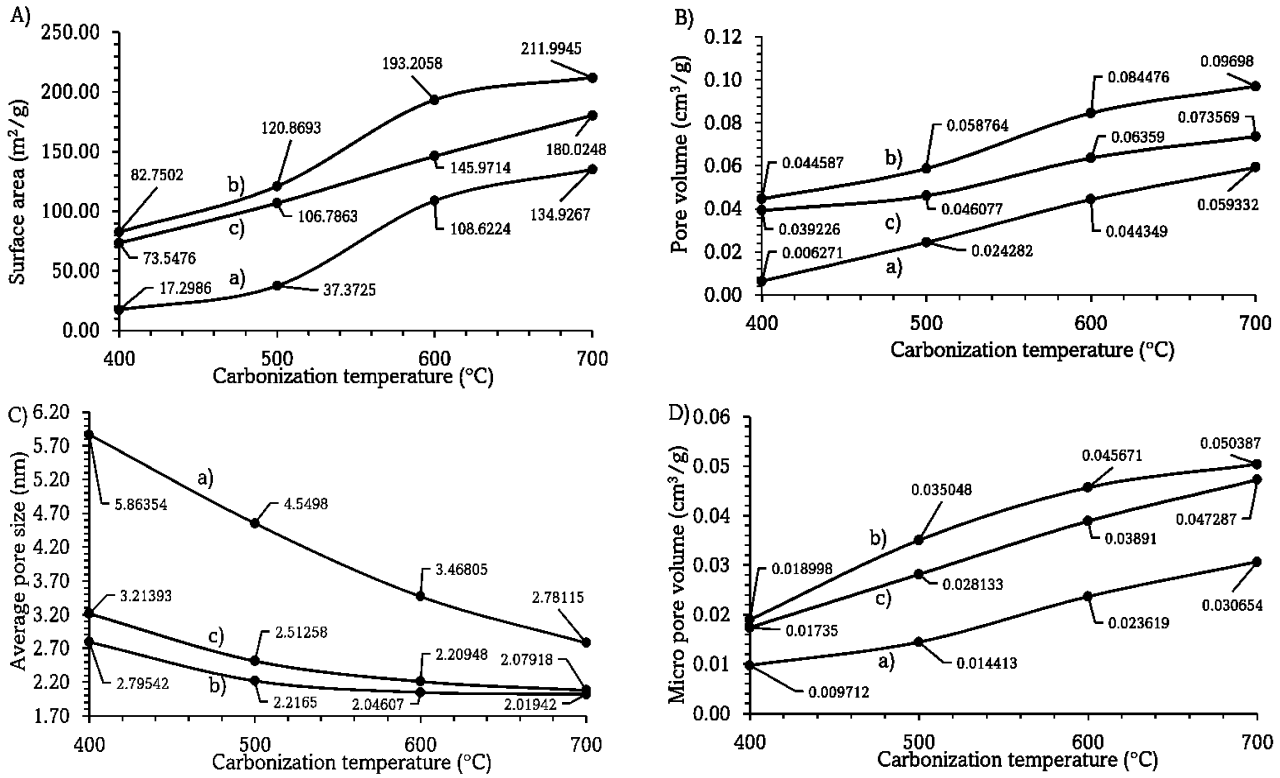

Fig 2. A) BET surface area, B) pore volume, C) pore size, and D) micro pore volume of a) cotton derived biochar fiber, b) Al-cotton derived biochar fiber, and c) Mg-cotton derived biochar fiber obtained at carbonization temperatures of 400°C-700°C.

activation process are significant. Furthermore, the effect of Al_2O_3 on all values is higher than the effect of $MgSO_4$. These results were attributed to the decomposition of organic compounds and vaporization of metal compounds at high temperatures with highly dispersed active sites and rapid mass transfer during carbonization (Xiao *et al*., 2023). Carbonization involving metal compounds activation involved chemical activation, which created more pores on the surface of the composite's products, and consequently, higher porosity with an improved surface area, pore volume, micropore volume, and average pore size (Hwang *et al*., 2021) compared to those of the biochar fiber made via carbonization without activation with metal compounds. Including, Al_2O_3 can react water or CO/CO_2 from organics decomposition during carbonization, which causes the partial destruction of surface carbon texture (Kaluža *et al*., 2022). While $MgSO_4$ has only affects the size of the microporous structure without generating a new porous structure (Zhou *et al*., 2018). Therefore, these values for the Al-cotton derived activated biochar fibers (Al- CABFs) are higher than the values for the Mg-cotton derived activated biochar fibers (Mg-CABFs), except for average pore sizes where the order is inverse. Including, this is because Al_2O_3 particles have porous morphology with high specific surface area and microporous structure (Urbonavicius *et al*., 2020). On the other hand, MgO particles were deposited in a film layer (Shang *et al*., 2021). Moreover, these trends levelled off for carbonization at temperatures between 600°C to 700°C of. This phenomenon is related to more severe reaction at high temperatures, resulting in serious external loss and the slow growth of micropores on the surfaces (Zhou *et al*., 2022) of the CBCFs and CABFs.

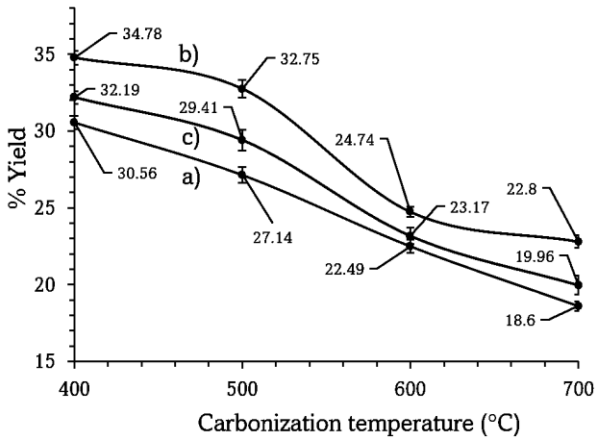

Fig 3. Percent yield of a) CBCFs, b) Al-CABFs, and c) Mg-CABFs made by carbonization at temperatures of 400°C-700°C.

3.2 Percent yield of products

The contents of fixed carbon, volatile matter, and ash determined by proximate analysis as a percentage of dried weight of CF are 30.28±0.53%, 69.41±0.82%, and 0.31±0.01%, respectively. This result showed that the percent yields of the CBCFs and CABFs may not exceed 35%. After the carbonization process, the percent yields of the CBCFs and CABFs decreased with increasing carbonization temperatures from 400°C to 700°C (Fig 3.a-c). This was attributed to the main thermal degradation of lignin during carbonization between 400°C and 700°C and some partial oxidation (Rattana-amron *et al*., 2024).

Higher carbonization temperatures provided more kinetic energy to break bonds of organic compounds leading to the expulsion of C, H, and O species in higher quantities, leading to the reduction of the yields of the residues (Khan *et al.*, 2022). In addition, the percent yields of the CABFs are higher than those of the CBCFs at all carbonization temperatures. This result is caused by numerous metal compound particles being embedded into the graphitic sheets of the CABFs (Costal *et al.*, 2021). Furthermore, the percent yields of the Al-CABFs are also higher than those of the Mg-CABFs. These results are attributed to the weight of Al_2O_3 in the final products. This is because of aluminium oxide is thermodynamically stable only losing the structural water and surface hydroxyl groups by desorption (Urbonavicius *et al.*, 2020). Furthermore, the dissociation of structural water and desorption of hydroxyl groups requited more heat. Therefore, the amount of heat for the carbonization process is decreasing (Özdemïr & Faruk Öksüzömer, 2020). On the other hand, the decomposition temperature of $MgSO_4$ is approximately 495°C and MgO is stable above 590°C (Souza *et al.*, 2020). In addition, it was also attributed to more extensive oxidation by some sulphate, which has remained in CF during carbonization between 400° and 700°C, of carbon texture of CF.

3.3 FTIR result of products

FTIR transmissions of the CBCFs prepared by carbonization at temperatures of 400°C-700°C are shown in Figs 4.a-d. The broad bands between 3250 cm^{-1}-3500 cm^{-1} correspond to hydroxyl groups, which are present in alcoholic, phenolic, and carboxylic derivatives formed from macromolecules such as cellulose, hemicellulose, and lignin (Guo *et al.*, 2018). Transmittance intensities of these bands decreased with increasing carbonization temperatures from 400°C to 700°C. Likewise, transmittance intensities of the weak double peaks at 2850 cm^{-1} and 2950 cm^{-1}, bands at 1420-1450 cm^{-1}, 1360-1390 cm^{-1}, and 1200-1230 cm^{-1} and a weak double peak at 820 and 890 cm^{-1} also decreased with increasing carbonization temperatures from 400°C to 700°C. These peaks and bands correspond to C-H asymmetric and symmetric stretching vibrations of aliphatic groups (Liu *et al.*, 2015), C-H in-plane bending of methyl and methylene groups (Guo *et al.*, 2018), aromatic C-O stretching vibrations of -COOH (Xu *et al.*, 2023), C-O-C stretching vibration of glycosyl ring in cellulose and hemicellulose (Guo *et al.*, 2018), and C-O stretching of aromatic ethers and esters (Thummajitsakul & Silprasit, 2022), respectively. Transmittance intensities of these functional groups gradually decreased with increasing temperature from 400°C to 700°C, which showed the decomposition of these functional groups and their release as volatiles. Furthermore,

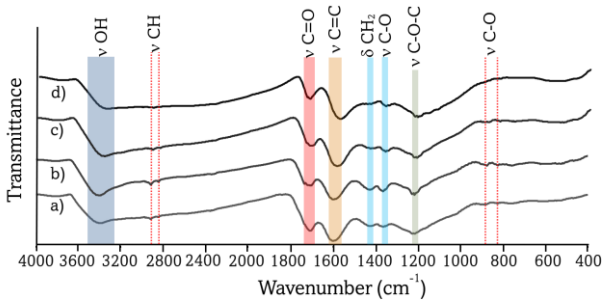

Fig 4. FTIR transmittance of CBCFs prepared by carbonization at temperature of a) 400°C, b) 500°C, c) 600°C, and d) 700°C.

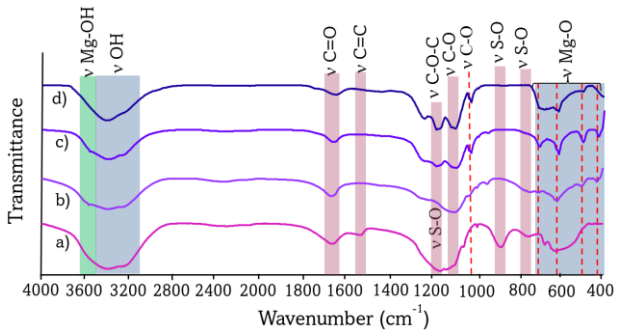

Fig 5. FTIR transmittance of Mg-CABFs made with carbonization at temperatures of a) 400°C, b) 500°C, c) 600°C, and d) 700°C.

these functional groups of the CBCFs are almost decomposed at carbonization temperature of 700°C. This is confirmed by the disappearance of these peaks and broadening of some bands, which indicates that oxygen containing functional groups were removed at higher carbonization temperatures (Khan *et al.*, 2022). Finally, double bands appeared at 1700-1750 cm^{-1} and 1580-1620 cm^{-1} corresponding to C=O stretching vibration of nonconjugated and conjugated carbonyl groups of those macromolecules in functional groups such as ester, ketone, carboxylic derivatives, and C=C stretching vibration of aromatic ring of lignin (Guo *et al.*, 2018), respectively. The band at 1580-1620 cm^{-1} is also related to C-O or C=O stretching vibration corresponding to functional groups like alcohols, esters, ethers, carboxylic acids, aldehydes, ketones, and carboxyl groups (Hasana *et al.*, 2021). Furthermore, it was seen that the band at 1700-1750 shifted to higher frequency, while the band at 1580-1620 cm^{-1} shifted to lower frequency with increasing carbonization temperature. This indicated that the aromaticity of the CBCFs was augmented (Sun *et al.*, 2023). In addition, apparent increase in the baseline transmission across the entire spectral region for CBCFs prepared at higher temperatures (600°C and 700°C) suggests a production of some graphitic carbon in nature (Li *et al.*, 2024), which have some oxygen containing functional groups (-OH, C=O, COOH and C-O-C), which remained from the starting material or were newly created under partial air oxidation.

FTIR transmission of the Mg-CABFs, which were activated with 5%wt. $MgSO_4$ using carbonization temperatures of 400-700°C, are shown in Fig 5.a-d. It can be seen that the bands of $Mg(OH)_2$ (relatively board band at 3400-3650 cm^{-1}; Hu *et al.*, 2023), which overlapped with bands of OH stretching, Mg-O (peaks between 420 cm^{-1} and 700 cm^{-1} (Hasana *et al.*, 2021), and -SO_4^{2-} groups [bands at about 1151-1180 cm^{-1}, 850-900 cm^{-1}, and 710-780 cm^{-1} (Sulaiman *et al.*, 2017)], are present in all

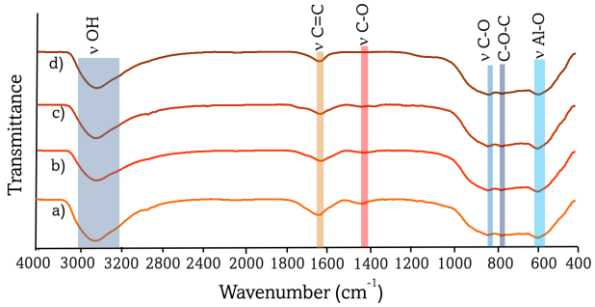

Fig 6. FTIR transmittance of Al-CABFs made with carbonization at temperatures of a) 400°C, b) 500°C, c) 600°C, and d) 700°C

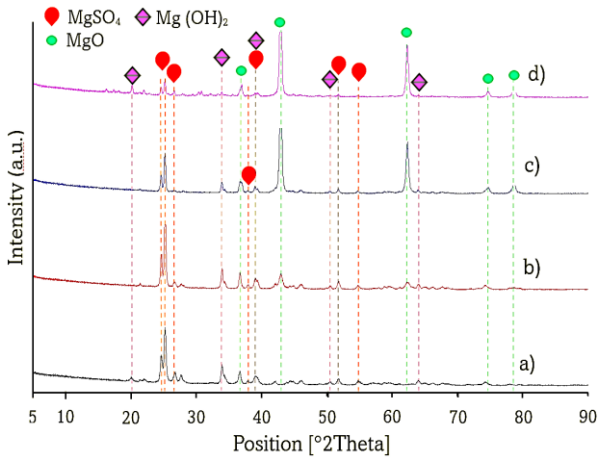

Fig 7. XRD patterns of Mg-CABFs prepared with carbonization at a) 400°C, b) 500°C, c) 600°C and d) 700°C.

spectra. This confirms that Mg accumulated on the cotton carbon fibers. However, the sulphate group disappeared after carbonization at 500°C. Furthermore, the breadth of the Mg-OH band has narrowed in response to increasing of the carbonization temperature from 400°C to 700°C, while the intensities of the Mg-O peaks tend to increase. This is due to the increase in MgO content in the CABFCs as a result of increasing carbonization temperature, which corresponded to the report of Sulaiman *et al.* (2017). The intensities of the bands at about 1510-1560 cm^{-1}, which correspond to aromatic C=C bonds, were significantly decreased, or even disappeared, after carbonization at 400-700°C. This is due to the formation of MgO, which coated the aromatic structure (Xiao *et al.*, 2024). Mg particles can be formed on the surface of the CABFs by attraction between the negatively charged surface of the CABF and the positively charged Mg ions, which facilitates the coating process of the surface of Mg-CABFs (Hasana *et al.*, 2021). During carbonization, the $MgSO_4$ was dissolved with SO_2 gas evolution and the formation of a surface precipitate of MgO and $Mg(OH)_2$ (Saleh & Hedia, 2018). The very broad bands for the O-H stretching vibration in the FTIR spectra of the Al-CABFs at about 3200-3600 cm^{-1} have also appeared with Al_2O_3 activation (Fig 6.a-d). The broadness of these bands lowered with increasing carbonization temperature from 400°C to 700°C. This is due to the higher dehydration at higher temperatures. The bands at about 1610-1650 cm^{-1} corresponding to stretching of C=C bonds in aromatic groups also exhibit lower intensities of transmission. In addition, C-O and C-O-C groups lead to bands with relatively low intensities of transmission. This is especially case for the peaks of C-O bond stretching (1400-1430 cm^{-1}), which disappeared after carbonization at 700°C. While the intensities of bands at about 550-600 cm^{-1}, which were attributed to the vibration of Al-O in Al_2O_3 (Ameen *et al.* 2024), are present in all spectra. This confirmed the presence of Al_2O_3 particles on the Al-CABFs surface with carbonization at temperatures of 400°C to 700°C. These functional groups act as a direct adsorption site (reversible or irreversible) in the spillover process, enhancing the formation of an island of the spilled-over H atoms around the oxygen groups and facilitating the surface diffusion and favorable adsorption of the atomic hydrogen (Sultana *et al.*, 2021). For -OH, C-O, C=O, COOH and C-O-C surface oxygen functional groups on the surface of CBCFs, Mg-CABFs, and Al-CABFs, these groups can enhance hydrogen spillover properties, resulting in a significant improvement in the hydrogen storage capacity of CBCFs, Mg-CABFs, and Al-CABFs (Shen *et al.*, 2022). However, these groups can also saturate the active carbon sites which leads to low physisorption of hydrogen (Bader *et al.*, 2018).

3.4 XRD results of products

The XRD diffractograms of the Mg-CABFs made by activation with $MgSO_4$ via carbonization at 400-700°C showed peaks of Mg, $MgSO_4$, $Mg(OH)_2$, and MgO (Figs 7.a-d). The intensities of peaks at 2θ= 24°, 25°, 27°, 38°, 52°, and 54.5°, which correspond to $MgSO_4$ (Okhrimenko *et al.*, 2020), decreased with increasing carbonization temperatures from 400°C to 700°C. It was seen that the XRD fractogram intensities of $MgSO_4$ are relatively high after carbonization at the temperatures of 400-500°C. This indicated that a high content of $MgSO_4$ remained in the produced materials. This is due to the high thermal requirements for the degradation of $MgSO_4$ to MgO, which takes place at about 998°C under oxidative conditions and at about 495 °C under CO reducing conditions. Full decomposition takes place at 1100°C (Souza *et al.*, 2020). On the contrary, the peaks at 2θ= 37°, 42.5°, 62.5°, 74.5°, and 78.5°, which correspond to MgO (Xiao *et al.*, 2024) increased with increasing carbonization temperatures from 400°C to 700°C. These results confirmed the formation of MgO by thermal decomposition of $MgSO_4$. It was seen that the conversion of $MgSO_4$ to MgO is initiated at 500°C under partial air oxidation and increased until 700°C leaving some residual content of $MgSO_4$ even at the highest temperature. This result is in accordance with the behaviour of the reaction $MgSO_4$ and charcoal system (Souza *et al.*, 2020). It was shown that the conversion of $MgSO_4$ to MgO is the main process under partial air oxidation. Furthermore, a small amount of $Mg(OH)_2$ was found in the products formed by carbonization at temperatures from 400°C to 700°C as indicated by peaks of very low intensities located at 2θ= 20°, 33°, 38°, 51.5°, and 64° (Kurosawa *et al.*, 2021), which became less intense in response to increasing carbonization temperatures from 400°C to 700°C. It was formed by chemical reaction between MgO and water (Kurosawa *et al.*, 2021), from dehydration of $MgSO_4$ hydrates and degradation of OH group in CF during carbonization. These results are in line with the FTIR results (Fig 5.) The XRD patterns of the Al-CABFs (Figs. 8.a-d) indicated that Al_2O_3 present in the products consisted almost entirely of γ-Al_2O_3 phase with a small amount of α-Al_2O_3

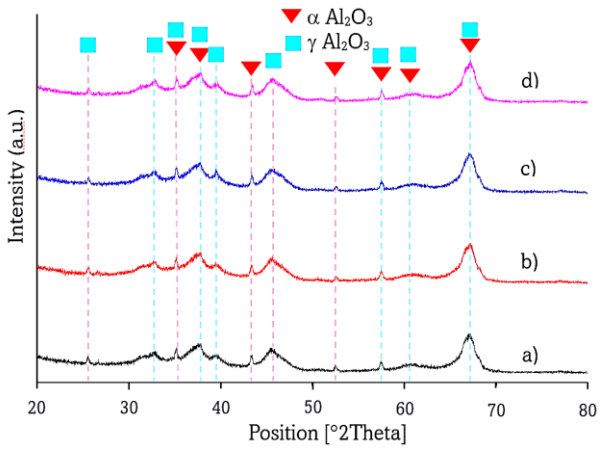

Fig 8. XRD patterns of Al-CABFs prepared with carbonization at a) 400°C, b) 500°C, c) 600°C, and d) 700°C.

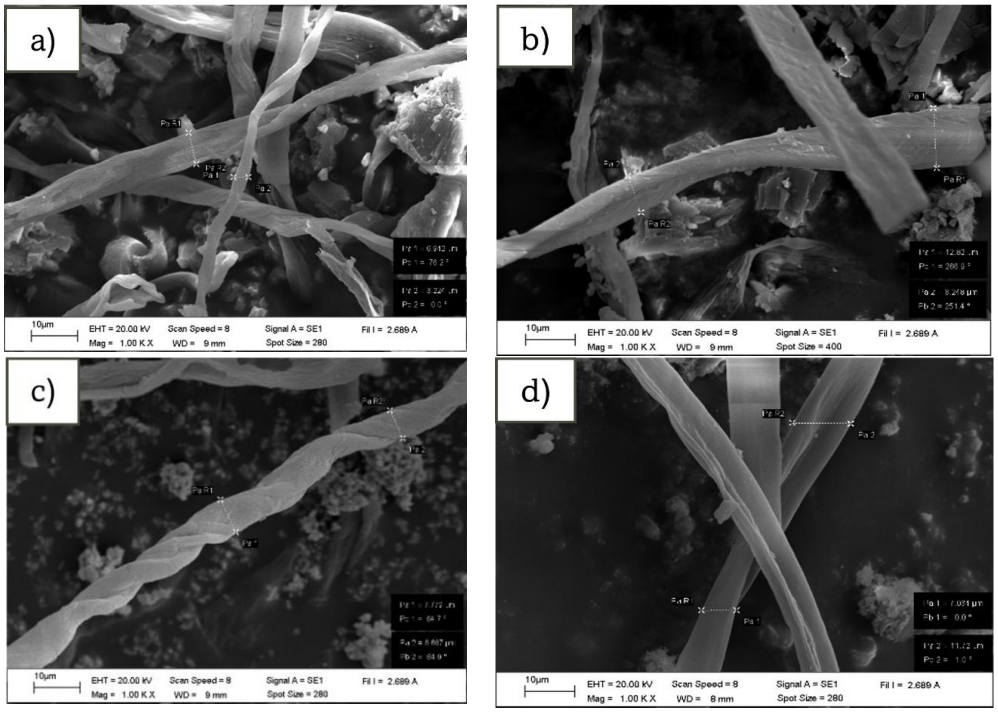

Fig 9. SEM morphologies of Mg-CABFs prepared with carbonization at temperatures of a) 400°C, b) 500°C, c) 600°C, and d) 700°C.

phase, which is consistent with the report of Suaebah *et al.* (2024). These results are also consistent with the FTIR results (Fig 6.). The formation of γ-Al_2O_3 phase was induced by thermal treatment at temperatures > 280°C with desorption of surface hydroxyl groups (Urbonavicius *et al.*, 2020). This desorption of surface hydroxyl groups led to lowering of broadness of the -OH bands as a result of increasing carbonization temperature from 400°C to 700°C (Fig 6.). The presence of both phases of Al_2O_3 were well-resolved and proved by the high intensity diffraction peaks in the XRD diffractogram (Ameen *et al.*, 2024), which depressed the diffractogram of graphite and amorphous carbon in the derived activated biochar fibers. It is even more interesting that the γ-Al_2O_3 phase has a large specific surface area and high chemical and thermal stability, and porous morphology (Urbonavicius *et al.*, 2020), which could lead to adsorption of hydrogen molecules. Therefore, both Mg-CABFs and Al-CABFs with support by non-reducible Al_2O_3 and MgO carriers

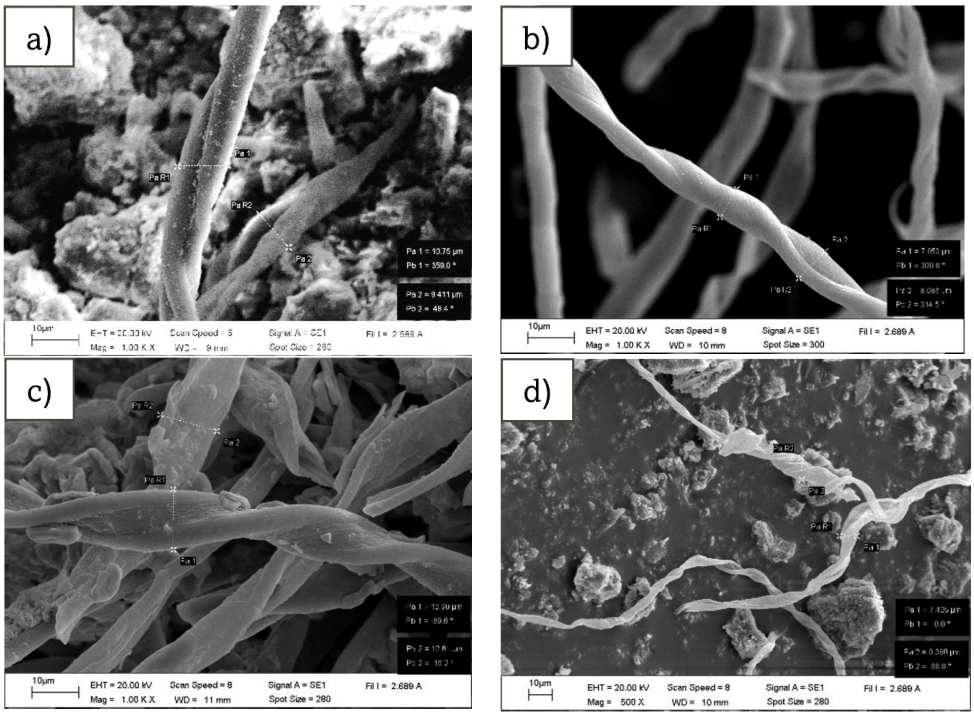

Fig 10. SEM morphologies of Al-CABFs prepared with carbonization at temperatures of a) 400°C, b) 500°C, c) 600°C, and d) 700°C.

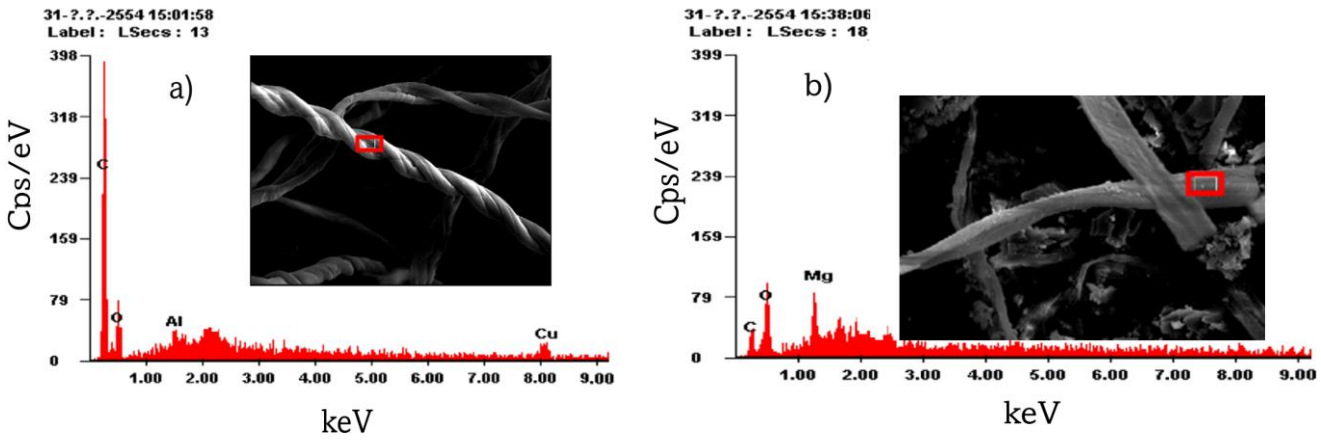

Fig 11. EDS spectra of a) Al-CABF, and b) Mg-CABF prepared with carbonization at 500°C.

for hydrogen spillover (Shen *et al.*, 2022). For Al_2O_3, active hydrogen substances can effectively spill on the surface of irreducible oxide Al_2O_3 due to the presence of defects and a small number of micropores as heating at high temperatures (Shen *et al.*, 2022). While the F centers (oxygen vacancies) in MgO, which generated defect, are formed in MgO after H_2 reduction at high temperature (Shun *et al.*, 2024). The effect of Al_2O_3 and MgO supports attributed to the basic/ionicity properties for diffusion of hydrogen spillover and transforming of the hydridic/protonic character of the resulting H atoms (Bettahar, 2024).

3.5 SEM morphology of products

SEM morphologies of the Mg-CABFs and Al-CABFs prepared using carbonization at 400°C-700°C are shown in Figs 9. and 10., respectively. The fibers of the products exhibit spiral shape of parallel fibrils and accumulated small particles on their surface. These parallel fibrils are closely packed after carbonization at 400°C (Figs 7.a and 8.a) and then have settled down at higher carbonization temperatures from 500°C to 700°C. These fibers showed open hollow nature after settling down and more extensive degradation with increasing carbonization temperatures from 400°C to 700°C (Figs 7.a-d and 8.a-d). This is ascribed to a more extensive expulsion of C, H, and O species at the higher carbonization temperatures (Khan *et al.*, 2022). The diameters of the fiber composites are approximately 7-13 μm with wrinkles, gullies, and hollow pores. These characteristics may be responsible in aiding the adsorption of hydrogen. These features could make the kinetics of hydrogen adsorption and desorption very fast and highly reversible since no structural change occurs in the framework (Hirscher *et al.*, 2020).

3.6 Elements composition from EDS

Energy dispersive spectroscopy (EDS) analysis results for the selected area (red square) on the surface of the CABFs are presented in Fig 11 (results shown only for materials prepared at 500°C). The elemental composition of the Mg-CABF is C, O, and Mg. In addition, the elemental composition of the Al-CABF is C, O, and Al. These results confirmed the successful incorporation of Mg (Fig 11.a) or Al (Fig 11.b) elements into CABFs, which is consistent with the results of the FTIR and XRD analyses.

3.7 Hydrogen storage results

The results of hydrogen adsorption of the CBCFs and CABFs have shown that hydrogen uptake capacity increased with increasing carbonization temperature from 400°C to 700°C used for the preparation of the CBCFs and CABFs (Fig 12). This is because the hydrogen uptake is proportional to the surface area, pore volume, and microporous character with condensation forces (Viswanathan, 2024). These characteristics are increased with increasing carbonization temperature from 400°C to 700°C, except microporous is inversed. In addition, more functional groups are present on the surfaces of the CBCFs and CABFs because of increasing of carbonization temperatures. These functional groups acted as receptors for spillover hydrogen by physisorption (Sharon *et al.*, 2011), which could improve the spillover efficiency and lead to an increase in the hydrogen storage capacity (Shen *et al.*, 2022). At the experimental conditions of 1.5 bar and room temperature, H_2 molecules were adsorbed on the functional groups with strong fluid–functional group interactions until they became saturated (Anuchitsakol *et al.*, 2023). In addition, the hydrogen uptake capacities of the CABFs (Figs 12.b and 12.c) are higher than those of CBCFs (Fig 12.a) prepared at the same carbonization temperatures. These results are attributed to the effects of accumulated metal compounds on surface of the CABFs, which acted as catalysts for enhancing the spill over mechanism for the hydrogen uptake capacity (Samantaray *et al.*, 2019). The metal compound particles are additives that act as a catalytic active center for the dissociation of hydrogen during the storage process, and the carbon receptor plays an important role as it provides the adsorption sites for the spillover of hydrogen (Sultana *et al.*, 2021). Furthermore, the hydrogen uptake capacities of the Al-CABFs (Fig 12.b) are higher than those of the Mg-CABFs (Fig 12.c) prepared at the same carbonization temperatures. This is because hydrogen can easily incorporate on top and bottom surfaces of Al_2O_3 (Gordon *et al.*, 2014). In addition, the γ-Al_2O_3 phase has a large specific surface area and porous morphology (Urbonavicius *et al.*, 2020). At the same time, the content of MgO films on the surface of the Mg-CABFs may be high and form a thick oxide layer, which leads to lower H_2 absorption rate (Shang *et al.*, 2021). Another reason is the effect of $Mg(OH)_2$ and $MgSO_4$ associated to H_2O, which has a negative effect on the hydrogen storage properties of Mg-based materials (Shang *et al.*, 2021). The H_2 capacity obtained in this study at room temperature and 1.5 bar fell within the range of 0.32-0.44 wt.%, 0.45-0.52 wt.%,

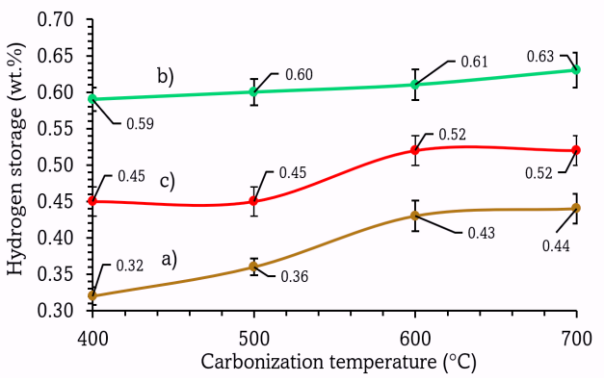

Fig 12. Hydrogen adsorption on a) CBCFs, b) Al-CABFs, and c) Mg-CABFs.

and 0.59-0.63 wt.% for the CBCFs, Mg-CABFs, and Al-CABFs, respectively. In addition, the doping of Al_2O_3 and MgO in the CABFs increased the hydrogen sorption capacities by 41.86%-66.67% and 18.18%-25.0%, respectively. In this study, hydrogen remains molecular and binds on the surface of the CBCFs and CABFs with physisorption. The main hydrogen adsorptions in this study are attributed to physisorption by microporous on surface of activated biochar products. The microporous are much more efficient in H_2 adsorption at lower pressures with the overlap of van der Waals potentials, which due to the atoms of adjacent walls favours stronger physisorption (Bader *et al.*, 2018). Therefore, hydrogen desorbs even at low temperatures (Viswanathan, 2024). Usually, the amounts of adsorbed hydrogen on industrial carbon adsorbents were no higher than 2 wt.% at room temperatures (20°C-30°C) and 200 bars, and the filling of the micropore volume was about 15%-20% (Fomkin *et al.*, 2021). However, hydrogen adsorptions in this study are quite good in comparison to MgO specimen and Al-MgO (1:5 ratio by weight) specimen), which can absorb 0.093 wt.% and 0.29 wt.% of hydrogen at air atmosphere pressure (1.01325 bar) and room temperature, respectively (Shun *et al.*, 2024). Another research, hydrogen storage for Al_2O_3 nanoparticle decorated functionalized multi-walled carbon nanotubes is range between 0.17 wt.% to 0.46 wt.% at 25°C and 70 bar (Konni & Mukkamala, 2019). Including, the MgO-activated fibers from polyacrylonitrile only adsorbed 0.7 wt.% H_2 at 50 bar and room temperature (Khafidz *et al.*, 2019). While the activated carbon material made with activation by KOH exhibited hydrogen uptake capacity of ~1.06 wt.% at 15 bar and 25°C (Samantaray *et al.*, 2019). In addition, 5 wt.% Ni on carbon nanospheres can adsorb hydrogen with capacity of only 0.42 wt.% at 50 bar and room temperature (Sharon *et al.*, 2011). In addition, they are still quite good as compared to commercial materials such as metal (e.g. Ni, Pt, Mg, Co, Zn)-organic frameworks (0.5–1 wt.% at room temperature and 100 bar), azine-linked covalent organic frameworks (0.99 wt.% at -196.15°C and 1 bar), boron-carbon nanotube (0.35 wt.% at 30°C and under 16 bar), graphene (0.25 wt.% at room temperature and 40 bars), nitrogen-enriched mesoporous carbons (0.03 wt.%-0.24 wt. at 25°C and 45 bar) (Osman *et al.*, 2024). It was seen that the Al-CABFs and the Mg-CABFs from CF by doped with Al_2O_3 and $MgSO_2$ and activated at 400°C-700°C can be considered as candidate adsorbers for hydrogen storage under 1.5 bar and room temperature with simplify practical process and low cost for commercial production, fast kinetics, quite high sorption selectivity/capacity, and sorption stability/reversibility.

4. Conclusion

Effects of carbonization temperature and activation with Al_2O_3 or $MgSO_4$ have a significant influence on the properties of the CBCFs and metal-CABFs. Surface areas and micropore volumes of these products are increased with increasing carbonization temperatures from 400°C to 700°C, while the trend for average pore sizes is inverted. In addition, Al_2O_3 or $MgSO_4$ exhibit beneficial effects on these properties with the effect of Al_2O_3 being higher than that of $MgSO_4$. This is because aluminium oxide is more thermodynamically stable than magnesium sulphate. These effects have caused the percent yield of products to have the same trend as the average pore sizes. The CBCFs have some oxygen containing functional groups such as -OH, C=O, COOH, and C-O-C on their surface. Mg-O and Al-O groups have occurred on the surface of the Mg-CABFs and Al-CABFs, respectively. This result is consistent with the XRD results, which show the presence of MgO and Al_2O_3 on the Mg-CABFs and Al-CABFs, respectively. These characteristics are confirmed by SEM-EDS results, which showed spiral shape of parallel fibrils with diameters of ~7-13 μm and accumulation of small particles on the surfaces. The Mg-CABFs and Al-CABFs showed open hollow nature after settling down and more extensive degradation with increasing carbonization temperature from 400°C to 700°C. The results of the investigation of hydrogen storage capacities show that hydrogen uptake capacity increased in proportion to surface area, pore volume, and microporous characteristics achieved with increasing carbonization temperature from 400°C to 700°C used for the preparation of the CBCFs and CABFs. The hydrogen adsorptions of the CBCFs and metal-CABFs are due to the action of surface functional groups as direct adsorption sites and the action of MgO or Al_2O_3 as catalytic active centers for enhancing the dissociation of hydrogen during the spillover process. It was shown that MgO and Al_2O_3 could improve the spillover efficiency leading to increase in the hydrogen storage capacity. Furthermore, the hydrogen uptake capacities of the Al-CABFs are higher than those of the Mg-CABFs for materials prepared at the same carbonization temperature. This result is attributed to the γ-Al_2O_3 phase in the Al-CABFCs, which has large specific surface area and porous morphology, while the MgO accumulated on the surface of the Mg-CABFs in the form of films and can be associated with H_2O. The hydrogen capacity obtained in this study at room temperature and 1.5 bar fell within the range of 0.32-0.44 wt.%, 0.45-0.52 wt.%, and 0.59-0.63 wt.% for the CBCFs, Mg-CABFs, and Al-CABFs, respectively. During the hydrogen storage by these products and under conditions of 1.5 bar and room temperature, hydrogen remains in its molecular form and binds on the surface of the CBCFs and CABFCs with physisorption. Therefore, hydrogen desorbs even at low temperature. This study can conclude that the Al-CABFs and Mg-CABFs from CF made by doping by Al_2O_3 and $MgSO_2$ and activation at 400-700°C are candidate adsorbers for hydrogen storage under 1.5 bar and room temperature with simplify practical process and low cost for commercial production, and also fast kinetics (within 30 min), quite high sorption selectivity/capacity (up 0.63 wt.%), and sorption stability/reversibility (at room temperature and 80°C).

Acknowledgments

This research was partially financially supported by Department of Chemistry, Faculty of Science, Naresuan University.

Author Contributions: S.M.: Conceptualization, methodology, formal analysis, writing-original draft, S.M.; supervision, resources, project administration, S.M.; writing-review and editing, project administration, validation, W.S.: writing-review and editing, project administration, validation. All authors have read and agreed to the published version of the manuscript.

Funding: No funding was received for conducting this study

Conflicts of Interest: The authors declare no conflict of interest.

References

Ameen, S., Hussain, Z., Din, M. I., Khan, R. U., & Khalid, R. (2024). Green synthesis of biochar@Al_2O_3 nanocomposite from waste melia azedarach fruit biomass pyrolysis: A sustainable solution for photocatalytic methylene blue dye degradation. *Desalination and Water Treatment,* 320, 100609; https://doi.org/10.1016/j.dwt.2024.100609

Anuchitsakol, S., Dilokekunakul, W., Khongtor, N., Chaemchuen, S., & Klomkliang, N. (2023). Combined experimental and simulation study on H_2 storage in oxygen and nitrogen co-doped activated carbon derived from biomass waste: superior pore size and surface chemistry development. *RSC Advances*, 13, 36009; https://doi.org/10.1039/d3ra06720c

ASTM (1998) *Standard Test Method for Volatile Matter Content of Activate Carbon*. ASTM D 5832-98. American Society for Testing and Materials, Pennsylvania.

ASTM (2011) *Standard Test Method for Total Ash content of Activate Carbon*. ASTM D 2866-11. American Society for Testing and Materials, Pennsylvania.

ASTM (2021) *Standard Practice for Proximate Analysis of Coal and Coke*. ASTM D3172-13(2021)e1. American Society for Testing and Materials, Pennsylvania.

Awais, H., Nawab, Y., Amjad, A., Anjang, A., Md Akil, H., & Abidin, M. S. Z. (2021). Environmental benign natural fibre reinforced thermoplastic composites: A review. *Composites Part C*, 4, 100082; https://doi.org/10.1016/j.jcomc.2020.100082

Bader, N., Zacharia, R., Abdelmottaleb, O., & Cossement, D. (2018). How the activation process modifies the hydrogen storage behavior of biomass-derived activated carbons. *Journal of Porous Materials,* 25, 221–234; https://doi.org/10.1007/s10934-017-0436-8

Buaki-Sogó, M., Zubizarreta, L., García-Pellicer, M., & Quijano-López, A. (2020). Sustainable carbon as efficient support for metal-based nanocatalyst: Applications in energy harvesting and storage. *Molecules*, 25(14), 3123; https://doi.org/10.3390/molecules25143123

Costal, G. Z., Oliveira, C. E. M., Morais, E. A. de., Oliveira, C. A. de S., Silva, E. E. da., Filho, F. M., & Geraldo, V. (2021). High-yield synthesis of carbon nanotubes in-situ on iron ore tailing. *Carbon Trends*, 5, 100098; https://doi.org/10.1016/j.cartre.2021.100098

Fomkin, A., Pribylov, A., Men'shchikov, I., Shkolin, A., Aksyutin, O., Ishkov, A., Romanov, K., & Khozina, E. (2021). Adsorption-based hydrogen storage in activated carbons and model carbon structures. *Reactions*, 2, 209–226; https://doi.org/10.3390/reactions 2030014

Guo, T., Ma, N., Pan, Y., Bedane, A. H., Xiao, H., Eić, M., & Du, Y. (2018). Characteristics of CO_2 adsorption on biochar derived from biomass pyrolysis in molten salt. *The Canadian Journal of Chemical Engineering*, 96(11), 2352-2360; https://doi.org/10.1002/cjce.23153

Gutsanu, V., Petuhov, O., Ipate, A. M., Lisa, G., & Botnaru, M. (2023). Metal/carbon composites: Precursors for obtaining new sorbents-catalysts. *Colloid Journal*, 85, 871–888; https://doi.org/10.1134/S1061933X23600537

Hasana, N. H., Wahi, R., Yusof, Y., & Mubarak, N. M. (2021). Magnesium-palm kernel shell biochar composite for effective methylene blue removal: Optimization via response surface methodology. *Pertanika Journal of Science and Technology*, 29(3), 1451-1473; https://doi.org/10.47836/pjst.29.3.28

Hirscher, M., Yartys, V. A., Baricco, M., Bellosta von Colbe, J., Blanchard, D., Bowman, R. C., Broom, D. P., Buckley, C. E., Chang, F., Chen, P., Cho, Y. W., Crivello, J. C., Cuevas, F., David, W. I. F, de Jongh, P. E., Denys, R. V., Dornheim, M., Felderhoff, M., Filinchuk, Y., & Zlotea, C. (2020). Materials for hydrogen-based energy storage – past, recent progress and future outlook. *Journal of Alloys and Compounds*, 827, 153548; https://doi.org/10.1016/j.jallcom.2019.153548

Hu, B., Yan, N., Zheng, Z., Xu, L., Xie, H., & Chen, J. (2023). Recyclable magnesium-modified biochar beads for efficient removal of phosphate from wastewater. *Nanomaterials*, 13(6), 966; https://doi.org/10.3390/nano13060966

Hwang, S. H., Kim, Y. K., Seo, H. J., Jeong, S. M., Kim, J., & Lim, S. K. (2021). The enhanced hydrogen storage capacity of carbon fibers: The effect of hollow porous structure and surface modification. *Nanomaterials*, 11(7), 1830; https://doi.org/10.3390/nano11071830

Kaluža, L., Soukup, K., Koštejn, M., Karban, J., Palcheva, R., Laube, M., & Gulková, D. (2022). On stability of high-surface-area Al_2O_3, TiO_2, SiO_2-Al_2O_3, and activated carbon supports during preparation of NiMo sulfide catalysts for parallel deoxygenation of octanoic acid and hydrodesulfurization of 1-benzothiophene. *Catalysts*, 12(12), 1559; https://doi.org/10.3390/catal12121559

Khafidz, N. Z. Abd. K., Yaakob, Z., Timmiati, S. N., Lin, K. S., & Lim, K. L. (2019). Hydrogen sorption of magnesium oxide carbon nanofibre composite. *Malaysian Journal of Analytical Sciences*, 23(1), 60-70; https://doi.org/10.17576/mjas-2019-2301-08

Khan, A., Iftikhar, K., Mohsin, M., Ahmad, J., Sahar, N., Rovere, M., & Tagliaferro, A. (2022). Low temperature synthesis of carbon fibres from post-consumer textile waste and their application to composites: An ecofriendly approach. *Diamond and Related Materials*, 130, 109504; https://doi.org/10.1016/j.diamond.2022.109504

Konni, M., & Mukkamala, S. B. (2019). Synthesis and hydrogen storage performance of Al_2O_3 nanoparticle decorated functionalized multi-walled carbon nanotubes (Al_2O_3@f-MWCNTs). *Journal of the Indian Chemical Society*, 96, 269-274.

Kryazheva, Y. G, Anikeevaa, I. V., Trenikhina, M. V., Zapevalovaa, E. S., & Semenova, O. N. (2019). Synthesis of metal–carbon composites with transition metal nanoparticles distributed as metal core–graphite-like shell structures in the bulk of an amorphous carbon matrix. *Solid Fuel Chemistry*, 53(5), 289-293; https://doi.org/10.3103/S0361521919050069.m

Kurosawa, R., Takeuchi, M., & Ryu, J. (2021). Fourier-transform infrared and X-ray diffraction analyses of the hydration reaction of pure magnesium oxide and chemically modified magnesium oxide. *RSC Advances*, 11(39), 24292-24311; http://dx.doi.org/10.1039/D1RA04290D

Lan, G., Yang, J., Ye, R., Boyjoo, Y., Liang, J., Liu, X., Li, Y., Liu, J., & Qian, K. (2021). Sustainable carbon materials toward emerging applications. *Small Methods*, 5(5), 2001250; https://doi.org/10.1002/smtd.202001250

Lee, W. G. (2020). Synthesis of metal-carbon composite composed of expanded graphite and nanometal. *ECS Meeting Abstracts*, MA2020-02, 1141; https://doi.org/10.1149/MA2020-0271141mtgabs

Li, K., Zhu, Y., Cao, H., Zhang, H., Wu, Y., Li, X., Xu, Z., & Liu, Q. (2024). Graphite made from coal by high-temperature treatment: An insight into the nanometric carbon structural evolution. *Minerals*, 14(11), 1092; https://doi.org/10.3390/min14111092

Okhrimenko, L., Favergeon, L., Johannes, K., & Kuznik, F. (2020). New kinetic model of the dehydration reaction of magnesium sulfate hexahydrate: Application for heat storage. *Thermochimica acta*, 687, 178569; https://doi.org/10.1016/j.tca.2020.178569

Osman, A. I., Ayati, A, Farrokhi, M., Khadempir, S., Rajabzadeh, Amin R., Farghali, M., Krivoshapkin, P., Tanhaei, B., Rooney, D. W., & Yap, P. S. (2024). Innovations in hydrogen storage materials: Synthesis, applications, and prospects. *Journal of Energy Storage*, 95, 112376; https://doi.org/10.1016/j.est.2024.112376

Özdemïr, H., & Faruk Öksüzömer, M. A. (2020). Synthesis of Al_2O_3, MgO and $MgAl_2O_4$ by solution combustion method and investigation of performances in partial oxidation of methane. *Powder Technology*, 359, 107-117; https://doi.org/10.1016/j.powtec.2019.10.001

Rattana-amron, T., Laosiripojana, N., & Kangwansupamonkon, W. (2024). Thermal oxidative degradation behavior of extracted lignins from agricultural wastes: Kinetic and thermodynamic analysis. *Industrial Crops and Products*, 219, 119096; https://doi.org/10.1016/j.indcrop.2024.119096

Saleh, M. E., & Hedia, R. M. R. (2018). Mg-modified sugarcane bagasse biochar for dual removal of ammonium and phosphate ions from aqueous solutions. *Alexandria Science Exchange Journal*, 9(1), 74-91; https://doi.org/10.21608/asejaiqjsae.2018.5753

Samantaray, S. S., Mangisetti, S. R., & Ramaprabhu, S. (2019). Investigation of room temperature hydrogen storage in biomass derived activated carbon. *Journal of Alloys and Compounds*, 789, 800-804; https://doi.org/10.1016/j.jallcom.2019.03.110

Shen, H., Li, H., Yang, Z., & Li, C. (2022). Magic of hydrogen spillover: Understanding and application. *Green Energy and Environment*, 7(6), 1161-1198; https://doi.org/10.1016/j.gee.2022.01.013

Shun. K., Mori, K., Kidawara, T., Satoshi Ichikawa, S., & Yamashita, H. (2024). Heteroatom doping enables hydrogen spillover via H+/e− diffusion pathways on a non-reducible metal oxide. *Nature Communications*, 15, 6403; https://doi.org/10.1038/s41467-024-50217-z

Shang, Y., Pistidda, C., Gizer, G., Klassen, T., & Dornheim, M. (2021). Mg-based materials for hydrogen storage. *Journal of Magnesium and Alloys*, 9(6), 1837-1860; https://doi.org/10.1016/j.jma.2021.06.007

Sharon, M., Sharon, M., Kalita, G., & Mukherjee, B. (2011). Hydrogen storage by carbon fibers synthesized by pyrolysis of cotton fibers. *Carbon Letters*, 12(1), 39-43; https://doi.org/10.5714/CL.2011.12.1.039

Souvakon, C., Vorasingha, A., Mopoung, S., & Vongkunghae, A. (2011). Synthesis and characterization of dehydroannulene carbon allotrope apply for hydrogen fuel storage. *International Journal of Physical Sciences*, 6(6), 1477-1483; https://doi.org/10.5897/IJPS10.171

Souza, B., Souza, R. Santos, I., & Brocchi, E. (2020). MgSO4 carbothermic reductive decomposition to produce a highly reactive MgO powder. *Journal of Materials Research and Technology*, 9(2), 1847-1855; https://doi.org/10.1016/j.jmrt.2019.12.017

Suaebah, E., Yunata, E. E., & Wijaya, A. S. N. (2024). The sintering temperature effect of alumina (Al_2O_3) ceramic using the sol-gel method. *Journal of Physics: Conference Series*, 2900, 012044; https://doi.org/10.1088/1742-6596/2900/1/012044

Sulaiman, M., Che Su, N., & Mohamed, N. S. (2017). Sol-gel synthesis and characterization of β-$MgSO_4$:$Mg(NO_3)_2$–MgO composite solid electrolyte. *Ionics*, 23, 443–452; https://doi.org/10.1007/s11581-016-1854-3

Sultana, A. I., Saha, N., & Reza, M. T. (2021). Synopsis of factors affecting hydrogen storage in biomass-derived activated carbons. *Sustainability*, 13, 1947; https://doi.org/10.3390/su13041947

Sun, W., Bai, L., Chi, M., Xu, X., Chen, Z., & Yu, K. (2023). Study on the evolution pattern of the aromatics of lignin during hydrothermal carbonization. *Energies*, *16*(3), 1089; https://doi.org/10.3390/en16031089

Tao, Y., Feng, W., He, Z., Wang, B., Yang, F., Nafsun, A. I., & Zhang, Y. (2024). Utilization of cotton byproduct-derived biochar: a review on soil remediation and carbon sequestration. *Environmental Sciences Europe*, 36, 79; https://doi.org/10.1186/s12302-024-00908-7

Thummajitsakul, S., & Silprasit, K. (2022). Analysis of FTIR spectra, flavonoid content and anti-tyrosinase activity of extracts and lotion from garcinia schomburgkiana by multivariate method. *Trends in Sciences*, 19(18), 5780; https://doi.org/10.48048/tis.2022.5780

Urbonavicius, M., Varnagiris, S., Pranevicius, L., & Milcius, D. (2020). Production of gamma alumina using plasma-treated aluminum and water reaction byproducts. *Materials*, 13, 1300; https://doi.org/10.3390/ma13061300

Viswanathan, B. (2024). *Options for solid state hydrogen storage*. Indian Institute of Technology, Madras, pp 139.

Xiao, J., Long, H., He, X., Chen, G., Yuan, T., Liu, Y., & Xu, Q. (2024). Synthesis of MgO-coated canna biochar and its application in the treatment of wastewater containing phosphorus. *Water*, 16(6), 873; https://doi.org/10.3390/w16060873

Xiao, W., Cheng, M., Liu, Y., Wang, J., Zhang, G., Wei, Z., Li, L., Du, L., Wang, G., & Liu, H. (2023). Functional metal/carbon composites derived from metal–organic frameworks: Insight into structures, properties, performances, and mechanisms. *ACS Catalysis*, 13(3), 1759-1790; https://doi.org/10.1021/acscatal.2c04807

Xu, Z., Wang, Y., Wu, M., & Chen, W. (2023). Preparation of biochar derived from waste cotton woven by low-dosage $Fe(NO_3)_3$ activation: characterization, pore development, and adsorption. *Environmental Science and Pollution Research*, 30, 49523–49535; https://doi.org/10.1007/s11356-023-25820-0

Yadav, K., & Ray, N. (2023). Hydrogen adsorption and diffusion through two-dimensional aluminium: A first-principles investigation. Journal of Physics: Conference Series, 2518, 012018; https://doi.org/10.1088/1742-6596/2518/1/012018

Yao, J., Wang, L., Xie, D., Jiang, L, Li, J., & Fang, X. (2022). Nanocarbon-based catalysts for selective n.itroaromatic hydrogenation: A mini review. *Frontiers in Chemistry*, 10, 1000680; https://doi.org/10.3389/fchem.2022.1000680

Zaghloul, M. Y. M., Zaghloul, M. M. Y., & Zaghloul, M. M. Y. Z. (2021). Developments in polyester composite materials – An in-depth review on natural fibres and nano fillers. *Composite Structures*, 278, 114698; https://doi.org/10.1016/j.compstruct.2021.114698

Zhou, K., Li, L., Ma, X., Mo, Y., Chen, R., Li, H., & Li, H. (2018). Activated carbons modified by magnesium oxide as highly efficient sorbents for acetone. *RSC Advances*, 8(6), 2922-2932; http://dx.doi.org/10.1039/C7RA11740J

Zhou, L., Zhong, M. Q., Wang, T., Liu, J. X., Mei, M., Chen, S., & Li, J. P. (2022). Study on the pyrolysis and adsorption behavior of activated carbon derived from waste polyester textiles with different metal salts. *Materials*, 15(20):7112. https://doi.org/10.3390/ma15207112